

Enhancement of the superconducting transition temperature by Re doping in Weyl semimetal MoTe₂

Manasi Mandal,¹ Sourav Marik,¹ K. P. Sajilesh,¹ Arushi,¹ Deepak Singh,¹ Jayita Chakraborty,¹ Nirmal Ganguli,¹ and R. P. Singh^{1,*}

¹*Indian Institute of Science Education and Research Bhopal, Bhopal, 462066, India*

(Dated: August 1, 2018)

This work presents the emergence of superconductivity in Re substituted topological Weyl semimetal MoTe₂. Re substitution for Mo sites lead to a sizable enhancement in the superconducting transition temperature (T_c). A record high T_c at ambient pressure in a 1T'-MoTe₂ (room temperature structure) related sample is observed for the Mo_{0.7}Re_{0.3}Te₂ composition ($T_c = 4.1$ K, in comparison MoTe₂, shows a T_c of 0.1 K). The experimental and theoretical studies indicate that Re substitution is doping electrons and facilitates the emergence of superconductivity by enhancing the electron-phonon coupling and density of states at the Fermi level. Our findings, therefore, open a new way to further manipulate and enhance the superconducting state together with the topological states in 2D van der Waals materials.

I. INTRODUCTION

The exotic quantum states such as topological states [1–3], Dirac semimetals [4–7] and Weyl semimetals [8–10] have been extensively studied in recent years as the new frontier of solid-state physics and chemistry. In this context, two-dimensional (2D) transition metal dichalcogenides (TMDs, TMCh₂) have attracted tremendous interest due to their rich structural and intercalation chemistry, unusual quantum states, and promising potential applications [11–15]. Illustrative examples include topological field-effect transitions based on quantum spin Hall (QSH) insulators [16], extremely large magnetoresistance (in T_d - WTe₂) [13] and artificial van der Waals heterostructures [17] with high on/off current ratio in TMDs. At the same time, rich electron coupling interactions foster exotic states of matter such as charge density waves (CDW) and unconventional superconductivity (SC) in TMDs [18–20].

The intrinsic chemical flexibility and the electron interactions achieved through the van der Waals stacking are enhanced further by the structural polymorphism of TMDs. MoTe₂ is a unique example among TMDs with the richest collections of variations on a structural theme (the semiconducting trigonal prismatic 2H phase, the semimetallic monoclinic 1T' (Fig. 1) and orthorhombic T_d phase) [21–23]. It shows an inversion symmetric monoclinic (space group P2₁/m, 1T' phase) - non-centrosymmetric orthorhombic (space group Pmn2₁, T_d Phase) structural phase transition at 250 K. The orthorhombic T_d phase with broken inversion symmetry is predicted to be a type - II Weyl semimetal and allows to study the fundamentals of novel quantum prop-

erties such as topological surface state Fermi arcs and chiral anomaly induced negative magnetoresistance [24–28]. Very recently, superconductivity with a very low transition temperature (T_c) of 0.1 K was discovered in the orthorhombic T_d MoTe₂ [11]. However, interestingly the application of external physical pressure enhances the T_c dramatically and further a dome - shaped superconducting phase diagram was established. Therefore, besides the exotic type - II Weyl semimetallic state, the discovery of superconductivity in T_d MoTe₂ offers a fascinating opportunity to explore superconductivity and topological states by tuning the local structural distortion or by manipulating the chemical pressure.

On the lure of increasing the superconducting transition temperature and to find out the origin of superconductivity in MoTe₂, most of the studies were concentrated on the manipulation of chemical pressure by substituting the chalcogenide site (isovalent substitution). Indeed, significant enhancement of T_c is achieved by replacing Te with S and Se (highest $T_c = 2.5$ K for MoTe_{2-x}Se_x series [29] and 1.3 K for MoTe_{2-x}S_x series [30]), however, the choices are limited in this case. On the other hand, substitution on the Mo sites leads to the advent of several novel properties, such as an enhancement of thermopower near the critical region between the polar and nonpolar metallic phases was discovered in Mo_{1-x}Nb_xTe₂ (hole doping) [31]. Furthermore, Mo_{1-x}W_xTe₂ alloy system is a promising candidate for the development of phase change memory technology [32]. Nevertheless, superconductivity in Mo substituted MoTe₂ is still elusive.

In this paper, we show the emergence of superconductivity in Mo_{1-x}Re_xTe₂ phases. The dependence of T_c with composition (x) and electron doping in the structure is described here. Furthermore, combining the ac and dc susceptibility, resistivity and specific heat measurements

* rpsingh@iiserb.ac.in

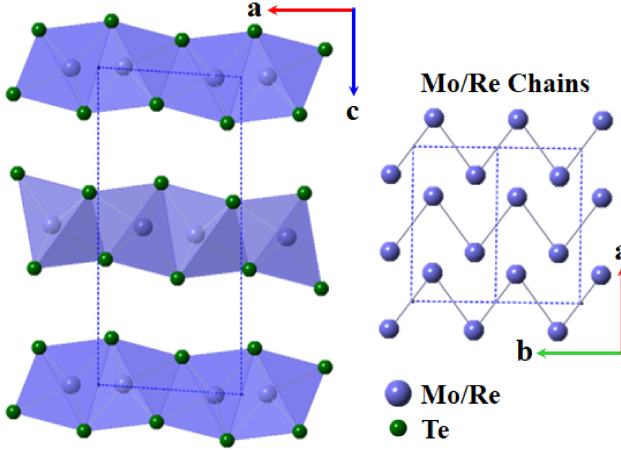


FIG. 1. Room temperature crystal structure of the $\text{Mo}_{1-x}\text{Re}_x\text{Te}_2$ materials (space group P21/m , $1\text{T}'$ phase). The zigzag Mo/Re chains along b direction are highlighted here.

we demonstrate that $\text{Mo}_{0.7}\text{Re}_{0.3}\text{Te}_2$ shows the highest $T_c = 4.1$ K at ambient pressure in a MoTe_2 related system.

II. EXPERIMENTAL DETAILS

Pure phase polycrystalline samples of composition $\text{Mo}_{1-x}\text{Re}_x\text{Te}_2$ ($x = 0, 0.05, 0.1, 0.2, 0.3$ and 0.4) were prepared by the standard solid-state reaction process. Stoichiometric mixtures of Mo (99.9% pure), Re (99.99% pure) and Te (99.99% pure) powders were ground together and sealed in an evacuated quartz tube. The ampoules were first heated at 1100°C for 24 hours. The obtained samples were then ground, pelletized, and annealed at 1100°C for 24 hours, followed by ice water quenching to avoid the formation of the 2H phases. Single crystals of composition $\text{Mo}_{0.9}\text{Re}_{0.1}\text{Te}_2$ was grown via chemical vapour transport method using polycrystalline $\text{Mo}_{0.9}\text{Re}_{0.1}\text{Te}_2$ powder and iodine as a transport agent. Crystals were obtained by sealing 3g of $\text{Mo}_{0.9}\text{Re}_{0.1}\text{Te}_2$ powder and I_2 in a quartz tube. The tube was then flushed with Ar, evacuated, sealed and heated in a two-zone furnace. Crystallization was carried out from 1100°C (hot zone) to 1000°C (cold zone) for 14 days. Finally, the sealed quartz tube was quenched in ice water to avoid the formation of the hexagonal phase. Powder X-ray diffraction (XRD) was carried out at room temperature (RT) on a PANalytical diffractometer equipped with $\text{Cu-K}\alpha$ radiation ($\lambda = 1.54056 \text{ \AA}$). Sample compositions were checked by a scanning electron microscope (SEM) equipped with an energy-dispersive X-ray (EDX) spectrometer. DC magnetization and ac susceptibility measurements were performed using a Quantum Design superconducting quantum interference device (MPMS 3, Quantum Design). The Hall measurements were car-

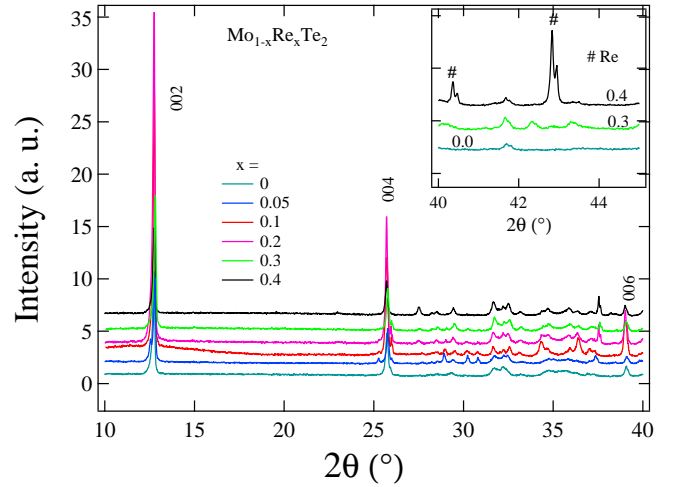


FIG. 2. Room temperature (RT) powder X-ray diffraction pattern for $\text{Mo}_{1-x}\text{Re}_x\text{Te}_2$ samples. Inset shows the unreacted Re peak in the XRD pattern for $x = 0.4$ sample.

ried out on the physical property measurement system (PPMS, Quantum Design, Inc.). Electrical resistivity measurements were performed on the PPMS by using a conventional four-probe ac technique at frequency 17 Hz and excitation current 10 mA. The measurements were carried out under the presence of different magnetic fields. Specific heat measurement was performed by the two tau time-relaxation method using the PPMS in zero magnetic field.

III. RESULTS AND DISCUSSION

Room temperature (RT) powder X-ray diffraction (XRD) patterns (Fig. 2) for the $\text{Mo}_{1-x}\text{Re}_x\text{Te}_2$ samples indicate that all the compounds can be isolated as single phase. However, an unreacted peak of Re in the RT XRD pattern is observed for the sample with $x = 0.4$ (inset in Fig. 2), and the intensity of the peak increases with increasing Re content in the nominal composition. At room temperature, all the samples crystallize in a centrosymmetric monoclinic structure (CdI_2 type, P21/m space group) consisting of edge-sharing (Mo/Re) Te_6 octahedra with a strong distortion (Fig. 1). The Energy-dispersive X-ray spectroscopy (EDX) analysis of the $\text{Mo}_{1-x}\text{Re}_x\text{Te}_2$ samples confirm the existence of Re, Mo and Te in the samples. Fig. 3 highlights the obtained amount of the Re in the structure for all the samples. EDX measurements were carried out at ten different points for each sample. The average of 10 points for each sample is shown in the Fig. 3 and this follows the nominal Re content. Therefore, within our experimental limit, we can say that the Re distribution in the samples is quite homogeneous. However, for the $x = 0.4$ sample the actual Re concentration is found to be smaller than the nominal one. This, in fact, supports the observation of the unreacted peaks

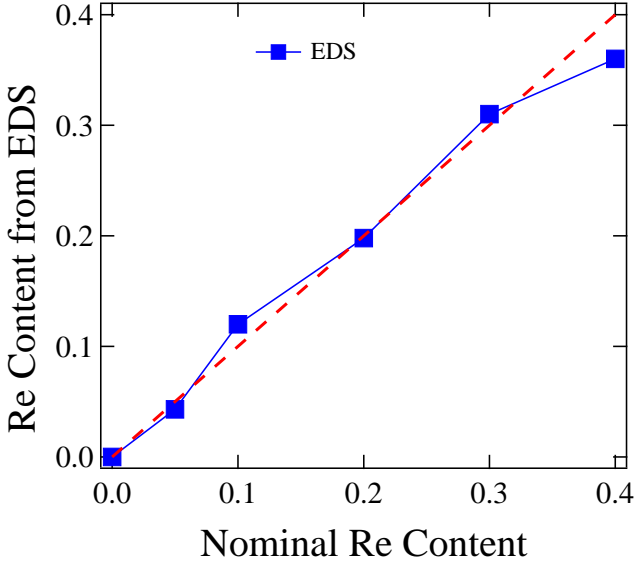


FIG. 3. Average Re concentration (average of 10 points) obtained from the EDX measurements for $\text{Mo}_{1-x}\text{Re}_x\text{Te}_2$ samples.

of Re in the RT XRD pattern for the $x = 0.4$ sample.

Also, we have grown the single crystal for $\text{Mo}_{0.9}\text{Re}_{0.1}\text{Te}_2$ composition. Fig. 4 (a) shows the RT XRD pattern on the naturally cleaved surface of the single crystal ([00l] reflections). Fig. 4 (b) shows the final plot of the Rietveld refinement of the powder XRD for $\text{Mo}_{0.9}\text{Re}_{0.1}\text{Te}_2$ crystals. EDX result shows that the average composition of our grown crystal is $\text{Mo}_{0.91}\text{Re}_{0.09}\text{Te}_2$. Temperature variation of the magnetic measurements on the crystal highlights superconducting transition at 3.2 K. Nevertheless, due to the low superconducting volume fraction in the crystals and the difficulty in processing (due to the small size), we have used the polycrystalline data in rest of the paper.

Fig. 5 shows the temperature dependence of resistivity for all the samples. The pristine MoTe_2 sample does not show superconducting state down to 1.8 K (T_d MoTe_2 shows SC at 0.1 K [11]), whereas the $x = 0.05$ sample exhibits a clear signature of superconducting state at 2.3 K. Interestingly, with increasing Re content in the structure, the superconducting transition temperature increases dramatically. $\text{Mo}_{0.7}\text{Re}_{0.3}\text{Te}_2$ ($x = 0.3$) shows a record high T_c of 4.1 K in any MoTe_2 related sample at ambient pressure. However, beyond this compositional point, T_c starts to decrease, and $x = 0.4$ sample shows lower onset T_c than $x = 0.3$. At the same time, the normal state resistivity highlights an anomalous behavior (broad hump) for the samples with $x = 0.2$ and 0.3 (inset in Fig. 5 (a)). The presence of a hump type anomaly in the resistivity data is not surprising for TMDs and may indicates the presence of a CDW state [33–35]. For instance, under high external pressure MoS_2 shows a similar hump type anomaly in the resistivity data due

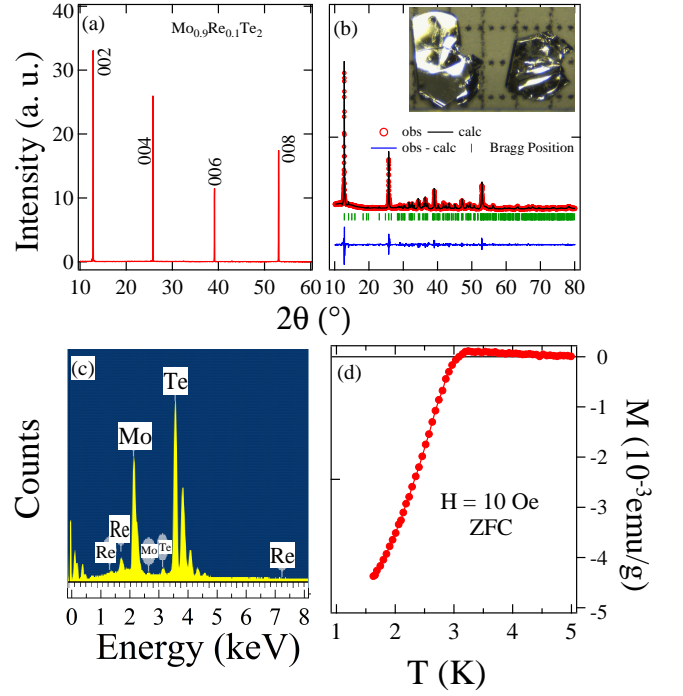


FIG. 4. (a) RT XRD pattern on the cleaved single crystal (b) the Rietveld refinement plots (c) EDX pattern and (d) temperature variation of the magnetic moment for $\text{Mo}_{0.9}\text{Re}_{0.1}\text{Te}_2$ crystals. Images of the grown crystals are shown in the inset of Fig 4(b).

to the existence of the CDW state [35]. Therefore, the observed anomaly in the normal state resistivity in our samples could be an indication of the appearance of the charge density wave (CDW) in the material. However, with further increasing the Re content in the structure metallic-type normal state behavior is observed. To verify the presence of CDW in the present materials, further experiments are required. The polar structural transition temperature (triangles in the Fig. 5 (a)), which is defined as the irreversibility (and an anomaly) between cooling and heating cycle of the resistivity data is found to decrease with increasing Re concentration. However, the irreversibility and the structural anomaly get weaker with Re doping and almost disappeared for samples with higher Re concentration ($x \geq 0.1$). Therefore, based on the present resistivity data it is not possible to precisely determine the Re-doping evolution of the structural transition. The enhanced superconducting states are characterized by dc and ac (Fig. 6) susceptibility measurements. Both the ac and dc susceptibility measurements confirm the evidence of bulk type - II superconductivity in Re doped MoTe_2 . The variation and the values of the T_c are consistent with the resistivity measurements. The lower critical field (H_{C1}) estimated from the isothermal magnetization curves are in the range of 20-50 Oe. Detailed study of the superconducting properties of the $\text{Mo}_{1-x}\text{Re}_x\text{Te}_2$ samples were carried out by measuring the resistivity and dc susceptibility under various applied

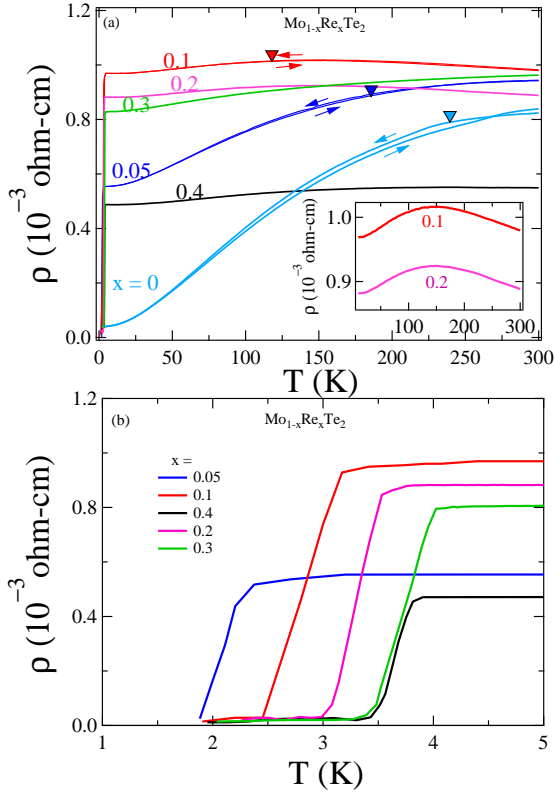


FIG. 5. Temperature dependence of (a) resistivity under zero magnetic field for $\text{Mo}_{1-x}\text{Re}_x\text{Te}_2$ samples. Solid triangles indicate the structural transition temperatures. Arrows highlight the cooling and heating process. Inset shows the observed anomaly in the normal state resistivity data for $x = 0.1$ and 0.2 samples. (b) Enlarged part of the resistivity measurements highlighting the superconducting transitions for $\text{Mo}_{1-x}\text{Re}_x\text{Te}_2$.

magnetic fields (H). The T_c is gradually suppressed with increasing magnetic field for all the samples (upper inset in Fig. 7). The temperature variation of the upper critical field (H_{C2}) for the samples is shown in Fig. 7. The critical temperatures are derived from the midpoint values of the superconducting transition in the resistivity measurements. The experimental H_{C2} can be described by the Ginzburg Landau expression.

$$H_{c2}(T) = H_{c2}(0) \frac{(1 - (T/T_c)^2)}{(1 + (T/T_c)^2)} \quad (1)$$

The estimated values of the upper critical field ($H_{C2}(0)$) show a gradual increment with increasing Re content in the structure. Interestingly, the upper critical field ($H_{C2}(0) = 7.2$ T) for the Re rich composition $\text{Mo}_{0.6}\text{Re}_{0.4}\text{Te}_2$ is found to be very close to the BCS weak coupling Pauli limit (7.23 T). In comparison, for the pristine MoTe_2 , $H_{C2}(0)$ value is far below the Pauli limit [11]. Therefore, the observed $H_{C2}(0)$ value for $\text{Mo}_{0.6}\text{Re}_{0.4}\text{Te}_2$, which is almost equal to the Pauli limit may points to the unconventional nature of the super-conductivity in the sample. The variation of Ginzburg Landau coherence

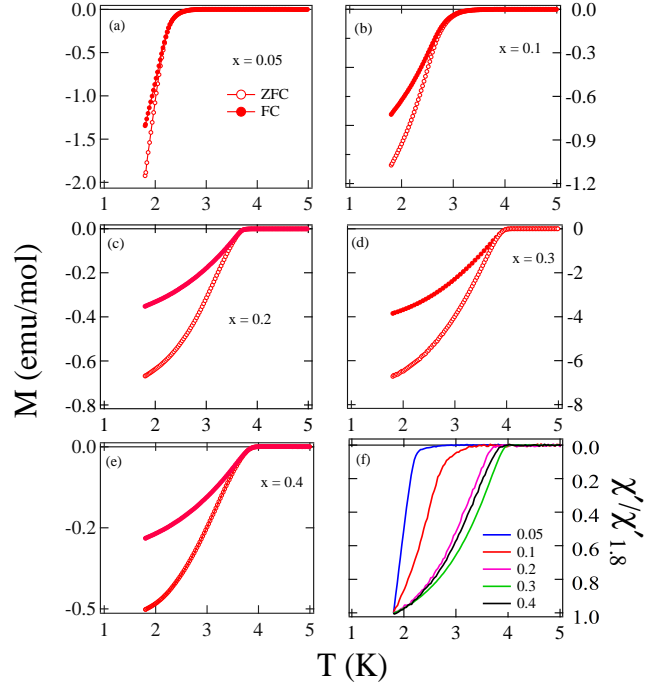


FIG. 6. Temperature dependence of (a)-(e) dc magnetization and (f) normalized ac susceptibility at a dc magnetic field of 10 Oe (ac excitation field = 2 Oe) for $\text{Mo}_{1-x}\text{Re}_x\text{Te}_2$ samples.

lengths $\xi_{GL}(0)$, estimated from the following relation, as a function of Re concentration is shown as an inset (lower inset) in Fig. 7.

$$H_{c2}(0) = \frac{\Phi_0}{2\pi\xi_{GL}^2} \quad (2)$$

The calculated values of $\xi_{GL}(0)$ are in the range of 6-11 nm and comparable with the $\xi_{GL}(0)$ value obtained for the pristine MoTe_2 under 11.2 GPa [11].

To determine the type of the charge carriers and its evolution with the Re substitution, we have measured the Hall resistivity for all the samples (Fig. 8). For the pristine MoTe_2 sample the magnetic field dependence of the Hall resistivity is curved with a negative slope, and this is typical of a semimetal having both hole and electron contributions. However, with increasing Re content in the material, the Hall profiles exhibit a straight-like behavior. This indicates that electron-like carriers are increasing with Re substitution. At the same time, a dramatic suppression of the magnetoresistance (MR, Fig. S3) is observed with Re substitution. It is noteworthy that in WTe_2 , superconductivity emerges due to the suppression of large magnetoresistance by the application of external pressure [36]. Upon increasing external pressure in WTe_2 , the electron concentrations start increasing and at a critical pressure of 10.5 GPa, superconductivity emerges with a change in the sign of the Hall coefficient (positive to negative) [36]. Fig. 9 summarizes the T_c and MR values for $\text{Mo}_{1-x}\text{Re}_x\text{Te}_2$ as a

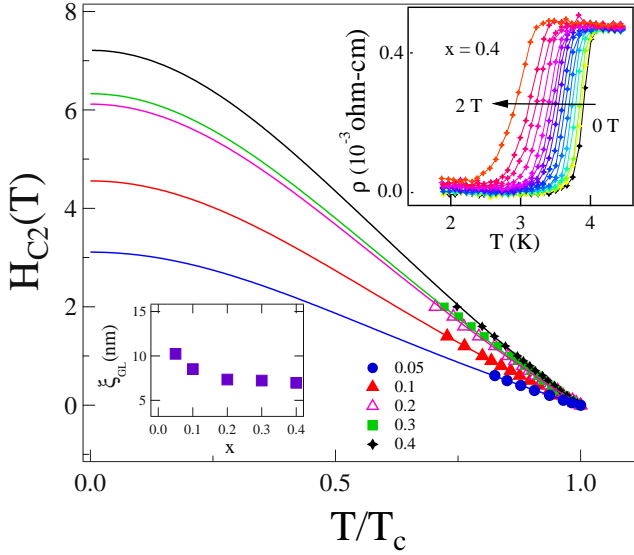


FIG. 7. Determination of the upper critical field ($H_{C2}(0)$) using resistivity measurements. The solid lines represent the Ginzburg Landau fitting. The upper inset shows the magnetic field variation of the resistivity for $x = 0.4$ sample. The Ginzburg Landau coherence length for the $\text{Mo}_{1-x}\text{Re}_x\text{Te}_2$ materials are shown in the lower inset.

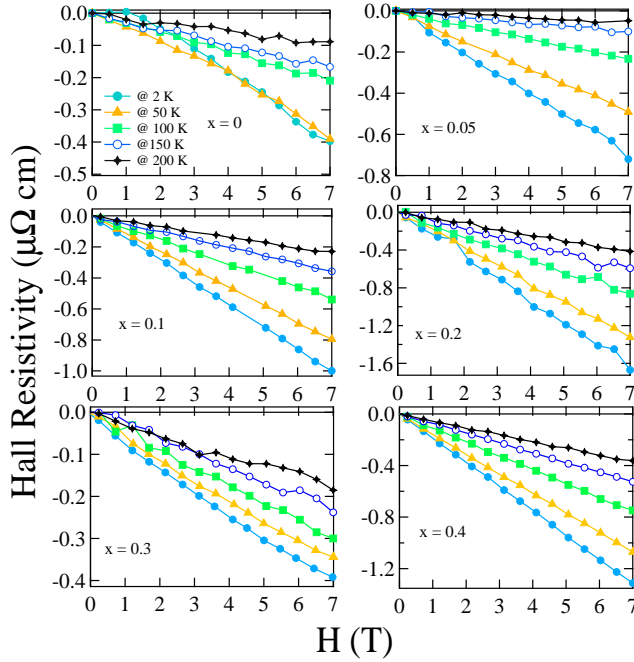


FIG. 8. Magnetic field variation of the Hall resistance at different temperatures for the $\text{Mo}_{1-x}\text{Re}_x\text{Te}_2$ samples.

function of Re concentration. This unambiguously highlights that the T_c dramatically increases with Re substitution of the Mo sites in MoTe_2 . On the contrary, Nb substituted MoTe_2 where Nb substitution induces holes in the structure do not exhibit superconductivity [31]. To analyze the phonon properties and electronic density of states of the non-SC and SC samples, we have performed

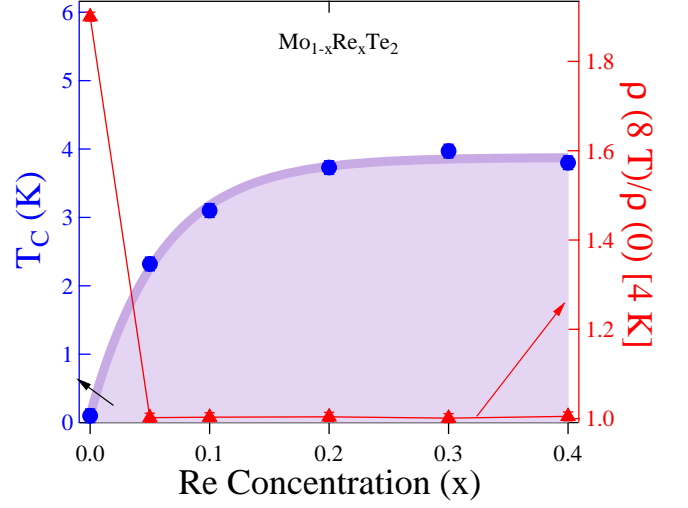


FIG. 9. The variation of the superconducting transition temperatures (T_c , left axis) and magnetoresistance (right axis) with Re substitution level in the structure for $\text{Mo}_{1-x}\text{Re}_x\text{Te}_2$.

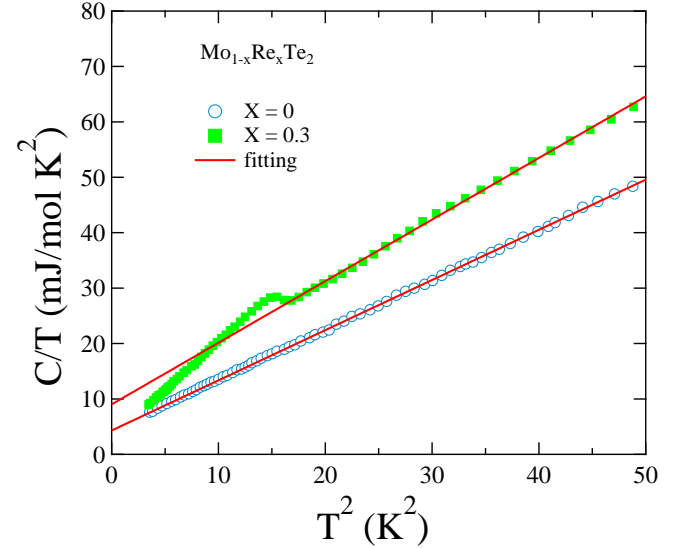


FIG. 10. The low-temperature specific heat data for MoTe_2 and for $\text{Mo}_{0.7}\text{Re}_{0.3}\text{Te}_2$. The specific heat data above T_c is fitted to the Debye model and shown by a solid line.

the heat capacity measurements for the $x = 0$ and 0.3 (highest T_c) samples. Fig. 10 illustrates the C_P/T as a function of T^2 above 1.8 K. The superconducting transition, which is manifested by a jump in the heat capacity data is observed at 4 K, confirming the bulk superconductivity in $\text{Mo}_{0.7}\text{Re}_{0.3}\text{Te}_2$. The low-temperature normal state specific heat can be extracted using the equation $C_P/T = \gamma + \beta T^2$ (γ = Sommerfeld coefficient and β is the lattice contribution to the specific heat) which yields $\gamma = 4.7$ and 9.0 mJ/mol K^2 for $x = 0$ and 0.3 respectively. Considering the free electron model, the density of states values at the Fermi level $[N(E_F) = \frac{3\gamma}{\pi^2 K_B^2}]$ is calculated as 2.01 and 3.83 states eV^{-1} f.u. $^{-1}$ for $x = 0$ and

0.3 respectively. The electron-phonon coupling constant, which gives the strength of the attraction between the electron and phonon can be calculated using the McMillan formula [37]

$$\lambda_{e-ph} = \frac{1.04 + \mu^* \ln(\theta_D/1.45T_c)}{(1 - 0.62\mu^*) \ln(\theta_D/1.45T_c) - 1.04} \quad (3)$$

By considering the Coulomb pseudopotential $\mu^* = 0.1$ [29], λ_{e-ph} are calculated as 0.31 and 0.64 for $x = 0$ and $x = 0.3$, respectively. These values indicate that the compounds are weak coupling superconductors. The increase in the electron concentration (by substituting the Re for Mo in MoTe_2) may facilitates the enhancement of the electron-phonon coupling and DOS at the Fermi energy. This, in fact, indicates that a significant reconstruction of the Fermi surface is occurring with Re substitution. The elementary density functional theory calculations [38] also indicates the enhancement of DOS. However, further experiments are required to gain deeper insights into Fermi surface reconstruction. The electron doping by means of Re substitution in the MoTe_2 phase shows the emergence of superconductivity, whereas the hole doping (Nb-doped MoTe_2 [31]) in MoTe_2 phase does not show superconductivity.

IV. CONCLUSION

In conclusion, we have successfully prepared a series of $\text{Mo}_{1-x}\text{Re}_x\text{Te}_2$ samples. Similar to the pristine 1T' MoTe_2 , at room temperature all the samples crystallize in a CdI_2 type centrosymmetric monoclinic structure (P21/m space group) consisting of edge-sharing (Mo/Re) Te_6 octahedra. The magnetic, transport and specific heat measurements highlight a dramatic enhancement of the superconducting transition temperature with Re substitution. Combining specific heat, Hall measurements indicate that the Re substitution is doping electrons. It can be a key reason to facilitates the emergence of superconductivity by enhancing the electron-phonon coupling and DOS at the Fermi energy. The estimated upper critical field ($H_{C2}(0) = 7.2$ T) for the Re rich composition $\text{Mo}_{0.6}\text{Re}_{0.4}\text{Te}_2$ is almost equal to the BCS weak coupling Pauli limit (7.23 T). It may be the indication of unconventional superconductivity. However, further experiments (such as Muon spectroscopy) are required to verify this point. A T_c , as high as 4.1 K is observed for the $\text{Mo}_{0.7}\text{Re}_{0.3}\text{Te}_2$ composition. In our best of knowledge, this is the highest T_c at ambient pressure, achieved yet in a 1T' MoTe_2 related sample. Unlike the pressure-enhanced superconducting state in Weyl semimetal MoTe_2 (and/or WTe_2), our findings open a new way to further manipulate and enhance the superconducting state together with the topological states in 2D van der Waals materials.

V. ACKNOWLEDGMENTS

R. P. S. acknowledges Science and Engineering Research Board (SERB), Government of India for the Young Scientist Grant No. YSS/2015/001799 and a Ramanujan Fellowship through Grant No. SR/S2/RJN-83/2012. S. M. acknowledges SERB, Government of India for the NPDF Fellowship (PDF/2016/000348). N. G. acknowledges SERB Grant No. ECR/2016/001004 and the use of HPC facility of IISER Bhopal. Financial support from DST-FIST Project No. SR/FST/PSI-195/2014(C) and DST-Nano Mission is also thankfully acknowledged

VI. CONTRIBUTIONS

M. M. and S. M. contributed this work equally.

-
- [1] H. J. Zhang, C. X. Liu, X. L. Qi, X. Dai, Z. Fang, S. C. Zhang, Nat. Phys. 5, 432-438 (2009).
 - [2] B. A. Bernevig, T. L. Hughes, S. C. Zhang, Science 314, 1757-1761 (2006).
 - [3] T. Kambe, R. Sakamoto, T. Kusamoto, T. Pal, N. Fukui, K. Hoshiko, T. Shimojima, Z. F. Wang, T. Hirahara, K. Ishizaka, S. Hasegawa, F. Liu, H. Nishihara, J. Am. Chem. Soc. 136, 14357-14360 (2014).
 - [4] Z. K. Liu, B. Zhou, Y. Zhang, Z. J. Wang, H. M. Weng, D. Prabhakaran, S.-K. Mo, Z. X. Shen, Z. Fang, X. Dai, Z. Hussain, and Y. L. Chen, Science 343, 864 (2014).
 - [5] S. M. Young, S. Zaheer, J. C. Y. Teo, C. L. Kane, E. J. Mele, and A. M. Rappe, Phys. Rev. Lett. 108, 140405 (2012).
 - [6] Z. Wang, Y. Sun, X.-Q. Chen, C. Franchini, G. Xu, H. Weng, X. Dai, Z. Fang, Phys. Rev. B 85, 195320 (2012).
 - [7] Z. Wang, H. Weng, Q. Wu, X. Dai, Z. Fang, Phys. Rev. B 88, 125427 (2013).
 - [8] B. Q. Lv, H. M. Weng, B. B. Fu, X. P. Wang, H. Miao, J. Ma, P. Richard, X. C. Huang, L. X. Zhao, G. F. Chen, Z. Fang, X. Dai, T. Qian, H. Ding, Phys. Rev. X 5, 031013 (2015).
 - [9] S.-Y. Xu, I. Belopolski, N. Alidoust, M. Neupane, G. Bian, C. Zhang, R. Sankar, G. Chang, Z. Yuan, C.-C. Lee, S.-M. Huang, H. Zheng, J. Ma, D. S. Sanchez, B. Wang, A. Bansil, F. Chou, P. P. Shihbayev, H. Lin, S. Jia, M. Z. Hasan, Science 349, 613 (2015).
 - [10] L. X. Yang, Z. K. Liu, Y. Sun, H. Peng, H. F. Yang, T. Zhang, B. Zhou, Y. Zhang, Y. F. Guo, M. Rahn, D. Prabhakaran, Z. Hussain, S.-K. Mo, C. Felser, B. Yan, Y. L. Chen, Nat. Phys. 11, 728 (2015).
 - [11] Y. Qi, P. G. Naumov, M. N. Ali, C. R. Rajamathi, O. Barkalov, Y. Sun, S. Chandra, S. -C. Wu, V. Suβ, M. Schmidt, P. Echhard, P. Werner, Reinald Hillebrand, F. Tobias, E. Kampertt, W. Schnelle, S. Parkin, R. J. Cava, C. Felser, B. Yan, S. A. Medvedev, Nat. Commun. 7, 11038 (2016).
 - [12] J. Guo, Y. Qi, S. Matsuishi, H. Hosono, J. Am. Chem. Soc. 134, 20001-20004 (2012)

- [13] M. N. Ali, J. Xiong, S. Flynn, J. Tao, Q. D. Gibson, L. M. Schoop, T. Liang, N. Haldolaarachchige, M. Hirschberger, N. P. Ong, R. J. Cava, *Nature* 514, 205-208 (2014)
- [14] J. Pan, C. Guo, C. Song, X. Lai, H. Li, W. Zhao, H. Zhang, G. Mu, K. Bu, T. Lin, X. Xie, M. Chen, F. Huang, *J. Am. Chem. Soc.* 139, 4623-4626 (2017).
- [15] R. Zhang, I-L. Tsai, J. Chapman, E. Khestanova, J. Waters, I. V. Grigorieva, *Nano Lett.* 16, 629-636 (2016).
- [16] X. Qian, J. Liu, L. Fu, J. Li, *Science* 346, 1344 (2014).
- [17] S. Cho, S. Kim, J. H. Kim, J. Zhao, J. Seok, D. HoonKeum, J. Baik, D.-H. Choe, K. J. Chang, K. Seunaga, S. W. Kim, Y. H. Lee, H. Yang, *Science* 349, 625 (2015).
- [18] B. Sipos, A. F. Kusmartseva, A. Akrap, H. Berger, L. Forro, E. Tutis, *Nature Mater.* 7, 960-965 (2008).
- [19] Y. I. Joe, X. M. Chen, P. Ghaemi, K. D. Finkelstein, G. A. de La Pena, Y. Gan, J. C. Lee, S. Yuan, J. Geck, G. J. MacDougail, T. C. Chiang, S. L. Cooper, E. Fradkin, P. Abbamonte, *Nature Phys.* 10, 421-425 (2014).
- [20] M. Calandra, F. Mauri, *Phys. Rev. Lett.* 106, 196406 (2011).
- [21] R. Clarke, E. Marseglia, H. P. Hughes, *Philos. Mag. B* 38, 121-126 (1978).
- [22] D. Puotinen, R. E. Newnhan, *Acta Crystallogr.* 14, 691-692 (1961).
- [23] T. Zandt, H. Dwelk, C. Janowitz, R. J. Manzke, *Alloys Compd.* 442, 216-218 (2007).
- [24] L. Fu, C. L. Kane, *Phys. Rev. Lett.* 100, 096407 (2008).
- [25] A. A. Soluyanov, D. Gresch, Z. Wang, Q. S. Wu, M. Troyer, X. Dai, B. A. Bernevig, *Nature* 527, 495-498 (2015).
- [26] Y. Sun, S.-C. Wu, M. N. Ali, C. Felser, B. Yan, *Phys. Rev. B* 92, 161107 (2015).
- [27] Z. Guguchia, F. von Rohr, Z. Shermadini, A. T. Lee, S. Banerjee, A. R. Wieteska, C. A. Marianetti, B. A. Frandsen, H. Luetkens, Z. Gong, S. C. Cheung, C. Baines, A. Shengelaya, G. Taniashvili, A. N. Pasupathy, E. Morenzoni, S. J. L. Billinge, A. Amato, R. J. Cava, R. Khasanov, Y. J. Uemura, *Nat. Commun.* 8, 1082 (2017).
- [28] X. Huang, L. Zhao, Y. Long, P. Wang, D. Chen, Z. Yang, H. Liang, M. Xue, H. Weng, Z. Fang, X. Dai, G. Chen, *Phys. Rev. X* 5, 031023 (2015).
- [29] H. Takahashi, H. Akiba, K. Imura, T. Shiino, K. Deguchi, N. K. Sato, H. Sakai, M. S. Bahramy, S. Ishiwata, *Phys. Rev. B* 95, 100501(R) (2017).
- [30] F. C. Chen, X. Luo, R. C. Xiao, W. J. Lu, B. Zhang, H. X. Yang, J. Q. Li, Q. L. Pei, D. F. Shao, R. R. Zhang, L. S. Ling, C. Y. Xi, W. H. Song, Y. P. Sun, *Appl. Phys. Lett.* 109, 102601 (2016).
- [31] H. Sun, Sakai, K. Ikeura, M. S. Bahramy, N. Ogawa, D. Hashizume, J. Fujioka, Y. Tokura, Ishiwata, S. *Science Advances* 2, e1601378 (2016).
- [32] S. M. Oliver, R. Beams, S. Krylyuk, I. Kalish, A. K. Singh, A. Bruma, F. Tavazza, J. Joshi, I. R. Stone, S. J. Stranick, A. V. Davydov, P. M. Vora, *2D Mater* 4, 045008 (2017).
- [33] E. Piatti, Q. Chen, M. Tortello, J. Ye, R. S. Gonnelli, *arXiv:1802.08449* (2018).
- [34] M. Naito, S. Tanaka, *J. Phys. Soc. Jpn.* 51, 219 (1982).
- [35] Zi-Yu Cao, Jia-Wei Hu, Alexander F. Goncharov, Xiao-Jia Chen, *Phys. Rev. B* 97, 214519 (2018).
- [36] D. Kang, Y. Zhou, W. Yi, C. Yang, J. Guo, Y. Shi, S. Zhang, Z. Wang, C. Zhang, S. Jiang, A. Li, K. Yang, Q. Wu, G. Zhang, L. Sun, Z. Zhao, *Nat. Commun.* 6, 7804 (2015).
- [37] W. L. Mcmillan, *Phys. Rev. B* 167, 331 (1968).
- [38] See Supplemental Material